

# Robust efficiency and actuator saturation explain healthy heart rate control and variability

Na Li<sup>a</sup>, Jerry Cruz<sup>b</sup>, Chenghao Simon Chien<sup>c,d</sup>, Somayeh Sojoudi<sup>e</sup>, Benjamin Recht<sup>f</sup>, David Stone<sup>g</sup>, Marie Csete<sup>h</sup>, Daniel Bahmiller<sup>b</sup>, and John C. Doyle<sup>b,c,i,1</sup>

<sup>a</sup>School of Engineering and Applied Sciences, Harvard University, Cambridge, MA 02138; <sup>b</sup>Department of Computing and Mathematical Science, California Institute of Technology, Pasadena, CA 91125; <sup>c</sup>Department of Electrical Engineering, California Institute of Technology, Pasadena, CA 91125; <sup>d</sup>Advanced Algorithm Research Center, Philips Healthcare, Thousand Oaks, CA 91320; <sup>e</sup>Department of Neurology, New York University Comprehensive Epilepsy Center, New York University School of Medicine, New York, NY 10016; <sup>f</sup>Department of Electrical Engineering and Computer Sciences and Department of Statistics, University of California, Berkeley, CA 94720; <sup>g</sup>Departments of Anesthesiology and Neurosurgery and the Center for Wireless Health, University of Virginia School of Medicine, Charlottesville, VA 22908; <sup>h</sup>Huntington Medical Research Institutes, Pasadena, CA 91101; and <sup>i</sup>Department of BioEngineering, California Institute of Technology, Pasadena, CA 91125

Edited\* by Michael S. Gazzaniga, University of California, Santa Barbara, CA, and approved June 27, 2014 (received for review January 30, 2014)

**The correlation of healthy states with heart rate variability (HRV) using time series analyses is well documented. Whereas these studies note the accepted proximal role of autonomic nervous system balance in HRV patterns, the responsible deeper physiological, clinically relevant mechanisms have not been fully explained. Using mathematical tools from control theory, we combine mechanistic models of basic physiology with experimental exercise data from healthy human subjects to explain causal relationships among states of stress vs. health, HR control, and HRV, and more importantly, the physiologic requirements and constraints underlying these relationships. Nonlinear dynamics play an important explanatory role—most fundamentally in the actuator saturations arising from unavoidable tradeoffs in robust homeostasis and metabolic efficiency. These results are grounded in domain-specific mechanisms, tradeoffs, and constraints, but they also illustrate important, universal properties of complex systems. We show that the study of complex biological phenomena like HRV requires a framework which facilitates inclusion of diverse domain specifics (e.g., due to physiology, evolution, and measurement technology) in addition to general theories of efficiency, robustness, feedback, dynamics, and supporting mathematical tools.**

system identification | optimal control | respiratory sinus arrhythmia

**B**iological systems display a variety of well-known rhythms in physiological signals (1–6), with particular patterns of variability associated with a healthy state (2–6). Decades of research demonstrate that heart rate (HR) in healthy humans has high variability, and loss of this high HR variability (HRV) is correlated with adverse states such as stress, fatigue, physiologic senescence, or disease (6–13). The dominant approach to analysis of HRV has been to focus on statistics and patterns in HR time series that have been interpreted as fractal, chaotic, scale-free, critical, etc. (6–17). The appeal of time series analysis is understandable as it puts HRV in the context of a broad and popular approach to complex systems (5, 18), all while requiring minimal attention to domain-specific (e.g., physiological) details. However, despite intense research activity in this area, there is limited consensus regarding causation or mechanism and minimal clinical application of the observed phenomena (10). This paper takes a completely different approach, aiming for more fundamental rigor (19–24) and methods that have the potential for clinical relevance. Here we use and model data from experimental studies of exercising healthy athletes, to add simple physiological explanations for the largest source of HRV and its changes during exercise. We also present methods that can be used to systematically pursue further explanations about HRV that can generalize to less healthy subjects.

Fig. 1 shows the type of HR data analyzed, collected from healthy young athletes ( $n = 5$ ). The data display responses to changes in muscle work rate on a stationary bicycle during mostly

aerobic exercise. Fig. 1A shows three separate exercise sessions with identical workload fluctuations about three different means. With proper sleep, hydration, nutrition, and prevention from overheating, trained athletes can maintain the highest workload in Fig. 1 for hours and the lower and middle levels almost indefinitely. This ability requires robust efficiency: High workloads are sustained while robustly maintaining metabolic homeostasis, a particularly challenging goal in the case of the relatively large, metabolically demanding, and fragile human brain.

Whereas mean HR in Fig. 1A increases monotonically with workloads, both slow and fast fluctuations (i.e., HRV) in HR are saturating nonlinear functions of workloads, meaning that both high- and low-frequency HRV component goes down. Results from all subjects showed qualitatively similar nonlinearities (*SI Appendix*). We will argue that this saturating nonlinearity is the simplest and most fundamental example of change in HRV in response to stressors (11, 12, 25) [exercise in the experimental case, but in general also fatigue, dehydration, trauma, infection, even fear and anxiety (6–9, 11, 12, 25)].

Physiologists have correlated HRV and autonomic tone (7, 11, 12, 14), and the (im)balance between sympathetic stimulation and parasympathetic withdrawal (12, 26–28). The alternation in autonomic control of HR (more sympathetic and less parasympathetic tone during exercise) serves as an obvious proximate cause for how the HRV changes as shown in Fig. 1, but the ultimate question remains as to why the system is implemented

## Significance

**Reduction in human heart rate variability (HRV) is recognized in both clinical and athletic domains as a marker for stress or disease, but previous mathematical and clinical analyses have not fully explained the physiological mechanisms of the variability. Our analysis of HRV using the tools of control mathematics reveals that the occurrence and magnitude of observed HRV is an inevitable outcome of a controlled system with known physiological constraints. In addition to a deeper understanding of physiology, control analysis may lead to the development of timelier monitors that detect control system dysfunction, and more informative monitors that can associate HRV with specific underlying physiological causes.**

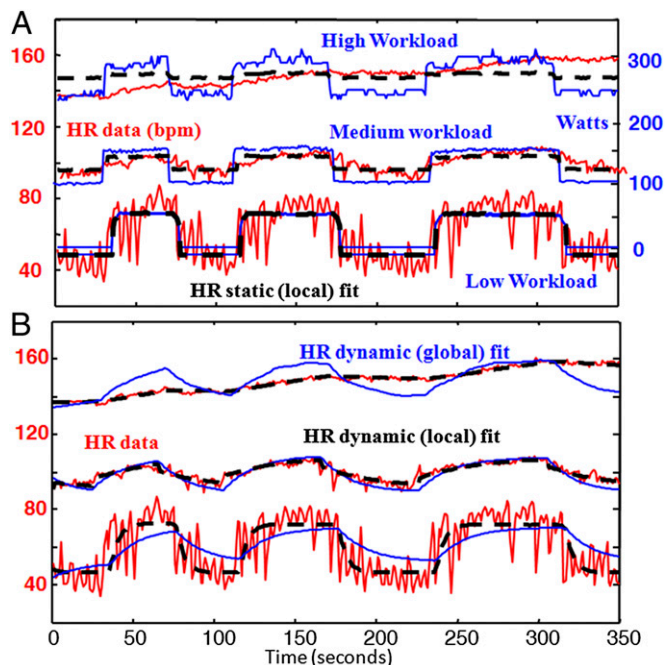
Author contributions: N.L., J.C., B.R., and J.C.D. designed research; N.L., J.C., C.S.C., B.R., D.B., and J.C.D. performed research; N.L., J.C., S.S., B.R., and J.C.D. contributed new reagents/analytic tools; N.L., J.C., C.S.C., S.S., and J.C.D. analyzed data; and N.L., D.S., M.C., and J.C.D. wrote the paper.

The authors declare no conflict of interest.

\*This Direct Submission article had a prearranged editor.

<sup>1</sup>To whom correspondence should be addressed. Email: doyle@caltech.edu.

This article contains supporting information online at [www.pnas.org/lookup/suppl/doi:10.1073/pnas.1401883111/-DCSupplemental](http://www.pnas.org/lookup/suppl/doi:10.1073/pnas.1401883111/-DCSupplemental).



whereas first-principles models give physiological interpretations to these dynamical relationships.

## Results

**Static Fits.** Table 1 lists the minimum root-mean-square (rms) error  $\|H_{data}-H_{fit}\|$  (where  $\|x\| = \sqrt{\sum_{t=1}^N (x_t)^2}/N$  for a time series  $x_t$  of length  $N$ ) for several static and dynamic fits of increasing complexity for the data in Fig. 1. Not surprisingly, Table 1 shows that the rms error becomes roughly smaller with increased fit complexity (in terms of the number of parameters). Rows 2 and 5 of Table 1 are single global linear fits for all of the data, whereas the remaining rows have different parameters for each cell and are thus piecewise linear when applied to all of the data. The “best” piecewise linear models balancing error with complexity are further highlighted in yellow in Table 1.

We will initially focus on static linear fits (first four rows) of the form  $h(W) = b \cdot W + c$ , where  $b$  and  $c$  are constants that minimize the rms error  $\|H_{data}-h(W)\|$ , which can be found easily by linear least squares. Static models have limited explanatory power but are simple starting points in which constraints and tradeoffs can be easily identified and understood, and we use only methods that directly generalize to dynamic models (shown later) with modest increase in complexity. Row 1 of Table 1 is the trivial “zero” fit with  $b = c = 0$ ; row 2 is the best global linear fit with  $(b, c) = (0.35, 53)$  which is used to linearly scale the units of  $W$  (blue) to best fit the HR data (red) in Fig. 1A; row 3 is a piecewise constant fit with  $b = 0$  and  $c$  being the mean of each data set; row 4 is the best piecewise linear fits (black dashed lines in Fig. 1A) with quite different values  $(b, c)$  of (0.44, 49), (0.14, 82), and (0.04, 137) at 0–50, 100–150, and 250–300 W. The piecewise linear model in row 4 has less error than the global linear fit in row 2. At high workload level, HR in Fig. 1 does not reach steady state on the time scale of the experiments, the linear static fit is little better than constant fit, and so these data are not considered further for static fits and models.

Both Table 1 and Fig. 1 imply that HR responds somewhat nonlinearly to different levels of workload stressors. The solid black curve in Fig. 3A shows idealized (i.e., piecewise linear) and qualitative but typical values for  $h(W)$  globally that are consistent with the static piecewise linear fits at the two lower watts levels in Fig. 1A. The change in slope of  $H = h(W)$  with increasing workload is the simplest manifestation of changing HRV and is now our initial focus. A proximate cause is autonomic nervous system balance, but we are looking for a deeper “why” in terms of whole system constraints and tradeoffs.

**Static Models.** As we mentioned earlier, in healthy fit subjects, the central physiological tradeoffs in cardiovascular control require keeping errors such as CBF,  $SaO_2$ , and  $\Delta O_2$  suitably small in response to variations in  $W$  disturbance through changes in actuations such as  $H$ . To better understand the tradeoff, we derive a steady-state model  $(P_{as}, \Delta O_2) = f(H, W)$  from standard physiology that constrains the relationship between  $(P_{as}, \Delta O_2)$  and  $(H, W)$  independent of how  $H$  is controlled (details below).

Here  $P_{as}$  is mean systemic arterial blood pressure, which is an important variable affecting the CBF (28, 38) and  $\Delta O_2$  is the drop in oxygen content across working muscle [Notice that the model already assumes constant  $SaO_2$ , which is consistent with data measurement and literature (27).] The mesh plot in Fig. 3C is the image on the  $(P_{as}, \Delta O_2)$  plane of the Fig. 3B  $(H, W)$  mesh plot under this function  $f(H, W)$  for generic, plausible values of physiological parameters (SI Appendix). Thus, any function  $H = h(W)$  can be mapped from the  $(H, W)$  plane using model  $(P_{as}, \Delta O_2) = f(H, W)$  to the  $(P_{as}, \Delta O_2)$  plane to determine its consequences for the most important tradeoffs, which involve  $P_{as}$  and  $\Delta O_2$ . These results are shown with the black lines in Fig. 3B, which give  $H = h(W)$  curves consistent with Fig. 3A and then are mapped onto Fig. 3C.

Hidden complexity is unavoidable in the model  $(P_{as}, \Delta O_2) = f(H, W)$ , but we temporarily defer these details to focus on the general shape of the color-coded curves in Fig. 3B and C, which have an intuitively clear explanation highlighted by the dashed red and purple lines. At constant workload, increased HR would greatly increase  $P_{as}$  while slightly decreasing  $\Delta O_2$  due to greater flow rate through the muscle. For constant HR, increased workload would greatly increase  $\Delta O_2$  while slightly reducing  $P_{as}$  due to greater oxygenation and peripheral vasodilatation. The cardiovascular control system adjusts HR as a function  $H = h(W)$  of workload to tradeoff increasing  $P_{as}$  with increasing  $\Delta O_2$ , both of which are undesirable. The modest curvature of the colored meshes in Fig. 3C demonstrates a small nonlinearity in the function  $(P_{as}, \Delta O_2) = f(H, W)$ . One source of this nonlinearity is the nonlinear relationship between cardiac output and HR due to less diastolic filling time as HR increases. However, the solid black lines in Fig. 3 manifest a much larger nonlinearity in the control function  $H = h(W)$ . We will argue that the essential sources of this nonlinearity are the tradeoff in robust homeostasis and metabolic efficiency and how it changes at different HR levels.

The hypothetical linear response at low workload in Fig. 3 can be explained in terms of purely metabolic tradeoffs. Healthy athletes can maintain the low workload almost indefinitely even in adverse (e.g., heat) conditions, a feature of human physiology thought to be an important adaptation for a successful hunter (39). Prolonged exercise necessarily requires steeply increased HR to provide sufficient tissue  $O_2$  (low  $\Delta O_2$ ), to maintain aerobic lipid metabolism in muscles and preserve precious carbohydrates for the brain.

The nonlinear response in Fig. 3 (solid lines) reflects additional tradeoffs that arise at higher workload and HR, when the resulting high  $P_{as}$  becomes dangerous mainly due to actuator saturation of cerebral autoregulatory control. In healthy humans, CBF is autoregulated to be quite constant (28, 38) over a relatively wide range of  $P_{as}$  ( $50 < P_{as} < 150$  mm Hg), so that no new tradeoffs at moderate exercise levels are required, because  $P_{as}$  is within this range. A new tradeoff does arise at  $P_{as}$  above 150 mm Hg when cerebral autoregulation saturates, and CBF begins to rise with the severe possible consequences of edema and/or hemorrhage. Thus, for the dashed black linear response in Fig. 3

**Table 1. rms error for models of different complexity for data in Fig. 1**

Row	No. parameters	Model structure	0–50 W	100–150 W	250–300 W
1	0	Zero: $h(W) = 0$	60.40	99.97	148.59
2	2	Global static: $h(W) = b \cdot W + c$	10.1	6.9	10.4
3	$3 = 1 \times 3$	Piecewise constant $h_i(W) = C_i$	14.8	4.7	6.7
4	$6 = 2 \times 3$	Piecewise static $h_i(W) = b_i \cdot W + C_i$	9.6	3.2	6.6
5	3	Global first order $\Delta h(t) = a h(t) + b W + c$	11.6	3.2	6.5
6	$9 = 3 \times 3$	Piecewise first order $\Delta h_i(t) = a h_i(t) + b_i W + C_i$	8.9	2.1	0.9

Items in yellow highlight the best models balancing fitting error with model complexity. For the piecewise model,  $i = 1, 2, 3$  stands for each exercise level, respectively; i.e., 0–50, 100–150, 250–300 W.



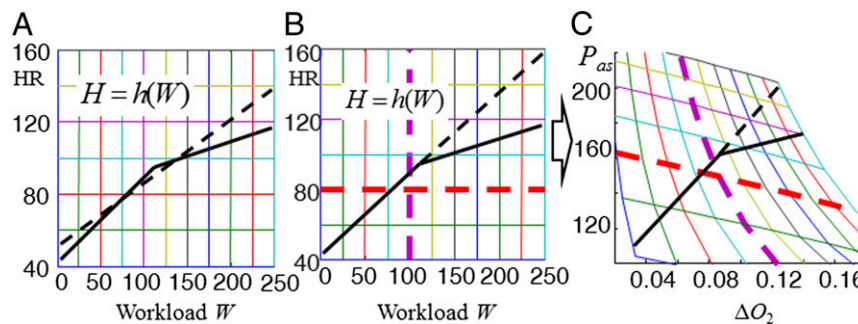


**Fig. 3.** Static analysis of cardiovascular control of aerobic metabolism as workload increases: Static data from Fig. 1A are summarized in A and the physiological model explaining the data is in B and C. The solid black curves in A and B are idealized (i.e., piecewise linear) and qualitatively typical values for  $H = h(W)$  that are globally consistent with static piecewise linear fits (black in Fig. 1A) at the two lower workload levels. The dashed line in A shows  $h(W)$  from the global static linear fit (blue in Fig. 1A) and in B shows a hypothetical but physiologically implausible linear continuation of increasing HR at the low workload level (solid line). The mesh plot in C depicts  $P_{as}-\Delta O_2$  (mean arterial blood pressure–tissue oxygen difference) on the plane of the  $H$ – $W$  mesh plot in B using the physiological model  $(P_{as}, \Delta O_2) = f(H, W)$  for generic, plausible values of physiological constants. Thus, any function  $H = h(w)$  can be mapped from the  $H, W$  plane (B) using model  $f$  to the  $(P, \Delta O_2)$  plane (C) to determine the consequences of  $P_{as}$  and  $\Delta O_2$ . The reduction in slope of  $H = h(W)$  with increasing workload is the simplest manifestation of changing HRV addressed in this study.

B and C, the resulting  $P_{as}$  would be elevated to potentially pathologic levels, and some nonlinearity as in the solid black line is necessary. Moreover, in many subjects there may be diminishing metabolic benefit of high tissue  $O_2$  (low  $\Delta O_2$ ) at high workloads because muscle mitochondria saturate. Although many details of cerebral autoregulation (as well as the mitochondrial saturation) are poorly understood, the  $P_{as}$  at which autoregulation saturates is well-known in healthy adults, and helps to explain an important change in HRV with stressors. Ultimately, cardiac output itself saturates at sufficiently high HR due to compromised diastolic filling time with subsequent dramatic falls in stroke volume.

Mathematically, all these factors can be quantitatively reflected in a static optimization model using linear least squares, with  $H = h(W)$  chosen to minimize a weighted penalty on increasing  $P_{as}$ ,  $\Delta O_2$ , and  $H$ :

$$\min q_P^2 (P_{as} - P_{as}^*)^2 + q_{\Delta O_2}^2 (\Delta O_2 - \Delta O_2^*)^2 + q_H^2 (H - H^*)^2$$

subject to linearization of the constraint  $(P_{as}, \Delta O_2) = f(H, W)$  at 0 and 100 W. Here  $P_{as}^*, \Delta O_2^*, H^*$  are the steady values for  $P_{as}, \Delta O_2, H$  at 0 and 100 W, respectively. Different values for  $(q_P, q_{\Delta O_2}, q_H)$  reflect different tradeoffs between  $P_{as}, \Delta O_2$ , and  $H$  at different workloads. In particular,  $q_P$  is higher at high workloads and high HR, reflecting the greater impact of  $P_{as}$  on CBF due to saturation of autoregulation, and  $q_H$  is higher to reflect the saturation of HR itself, which becomes more acute at higher workload levels. Straightforward, standard computations easily reproduce the piecewise linear features in Fig. 3 with higher penalty on  $P_{as}$  and  $H$  at higher workload levels.

An important feature of this approach is that it allows systematic exploration of models that are both simple and explanatory. We have systematically moved from the data in Fig. 1 to the fit in Fig. 3A, and then from very simple well-understood physiological mechanisms to how healthy HR should behave and be controlled, reflected in Fig. 3B and C. The nonlinear behavior of HR is explained by combining explicit constraints in the form  $(P_{as}, \Delta O_2) = f(H, W)$  due to well-understood physiology with constraints on homeostatic tradeoffs between rising  $P_{as}$  and  $\Delta O_2$  that change as  $W$  increases. The physiologic tradeoffs depicted in these models explain why a healthy neuroendocrine system would necessarily produce changes in HRV with stress, no matter how the remaining details are implemented. Taken together this could be called a “gray-box” model because it combines hard physiological constraints both in  $(P_{as}, \Delta O_2) = f(H, W)$  and homeostatic tradeoffs to derive a resulting  $H =$

$h(W)$ . If new tradeoffs not considered here are found to be significant, they can be added directly to the model as additional constraints, and solutions recomputed. The ability to include such physiological constraints and tradeoffs is far more essential to our approach than what is specifically modeled (e.g., that primarily metabolic tradeoffs at low HR shift priority to limiting  $P_{as}$  as cerebral autoregulation saturates at higher HR). This extensibility of the methodology will be emphasized throughout.

The most obvious limit in using static models is that they omit important transient dynamics in HR, missing what is arguably the most striking manifestations of changing HRV seen in Fig. 1. Fortunately, our method of combining data fitting, first-principles modeling, and constrained optimization readily extends beyond static models. The tradeoffs in robust efficiency in  $P_{as}$  and  $\Delta O_2$  that explain changes in HRV at different workloads also extend directly to the dynamic case as demonstrated later.

**Dynamic Fits.** In this section we extract more dynamic information from the exercise data. The fluctuating perturbations in workload (Fig. 1) imposed on a constant background (stress) are targeted to expose essential dynamics, first captured with “black-box” input–output dynamic versions of above static fits. Fig. 1B shows the simulated output  $H(t) = \text{HR}$  (in black) of simple local (piecewise) linear dynamics (with discrete time  $t$  in seconds)

$$\Delta H(t) = H(t+1) - H(t) = Hh(t) + bW(t) + c, \quad [1]$$

where the input is  $W(t) = \text{workload}$  (blue). Constants  $(a, b, c)$  are fit to minimize the rms error between  $H(t)$  and HR data as before (Table 1). The optimal parameter values  $(a, b, c) \sim (-0.22, 0.11, 10)$  at 0 W differ greatly from those at 100 W  $(-0.06, 0.012, 4.6)$  and at 250 W  $(-0.003, 0.003, -0.27)$ , so a single model equally fitting all workload levels is necessarily nonlinear. This conclusion is confirmed by simulating HR (blue in Fig. 1B) with one best global linear fit  $(a, b, c) \sim (0.06, 0.02, 2.93)$  to all three exercises, which has large errors at high and low workload levels.

The changes of the large, slow fluctuations in both HR (red) and its simulation (black) in Fig. 1B are consistent with well-understood cardiovascular physiology, and illustrate how the physiologic system has evolved to maintain homeostasis despite stresses from workloads. Our next step in modeling is to mechanistically explain as much of the HRV changes in Fig. 1 as possible using only standard models of aerobic cardiovascular physiology and control (27–31). This step focuses on the changes in HRV in the fits in Fig. 1B (in black) and Eq. 1, and we defer

modeling of the high-frequency variability in Fig. 1 until later (i.e., the differences between the red data and black simulations in Fig. 1B).

The black-box fits allow us to plausibly conjecture that workload disturbances cause most of the variability in Fig. 1B (black curves). Here the rigor of the black-box fits is important, as highlighted by three features: (i) no comparably good fits exist for the data in Fig. 1 without the input of workload, (ii) within the limits of the sensors used and subject fitness we can otherwise experimentally manipulate the input independently and over a wide range to make it truly a “causal” input, and (iii) the fits accurately predict the HR output response to new experiments (i.e., cross-validation; see *SI Appendix*).

**First-Principles Models.** Our first-principles model is based on the circulatory circuit diagram in Fig. 2, using standard mathematical descriptions of circulation, and with a focus on modeling purely aerobic exercise. That is, we only model blood flow, blood pressure, and O<sub>2</sub> in several compartments, and yet the model captures the overall physiologic HR response during moderate exercise in young, fit adults. In standard models of aerobic cardiovascular control (27–31) the neuroendocrine system controls peripheral vasodilation, minute ventilation, and cardiac output to maintain blood pressure and oxygen saturation within acceptable physiological limits.

Several features of these control systems allow substantial simplification of the model. Minute ventilation  $\dot{V}_E$  alone can tightly control arterial oxygenation  $[O_2]_a$ , so we assume  $[O_2]_a$  is maintained nearly constant (27). Moreover, peripheral resistance  $R_s$  is decreased during exercise and the decrease is determined by local metabolic control. The purpose of decreasing  $R_s$  in the arterioles is to increase blood flow and regional delivery of O<sub>2</sub>, glucose, and other substrates as needed. Because the venous oxygenation  $[O_2]_v$  serves as a good signal for oxygen consumption, we also assume that control of peripheral vascular resistance  $R_s$  is a function only of venous oxygenation  $[O_2]_v$  (31).

Combined with those models for blood circulation and oxygen consumption, we have the following physiological model:

$$\begin{aligned} V_{as} &= c_{as} \cdot P_{as} & Q_l &= c_l \cdot H \cdot P_{vp} \\ V_{vs} &= c_{vs} \cdot P_{vs} & Q_r &= c_r \cdot H \cdot P_{vs} \\ V_{ap} &= c_{ap} \cdot P_{ap} & F_s &= (P_{as} - P_{vs})/R_s \\ V_{vp} &= c_{vp} \cdot P_{vp} & F_p &= (P_{ap} - P_{vp})/R_p \\ V_{tot} &= V_{as} + V_{vs} + V_{ap} + V_{vp} & M &= \rho \cdot W + M_0 \\ [O_2]_a &= 0.2 & R_s &= A \cdot [O_2]_v + R_{s0}. \end{aligned} \quad [2]$$

Here  $V$  and  $P$  are (subscripts  $a$  = arterial,  $v$  = venous,  $s$  = systemic,  $p$  = pulmonary) blood volume and blood pressure, respectively. All of the  $c$  variables are constants. The main elements of the model are (more details in *SI Appendix*): (i) arterial and venous compartments of systemic and pulmonary circulations are treated as compliant vessels, modeled in the form  $V = c \cdot P$ , with the total blood volume a constant  $V_{tot}$ ; (ii) cardiac output of the left ( $Q_l$ ) and right ( $Q_r$ ) ventricles; (iii) blood flow for systemic ( $F_s$ ) and pulmonary ( $F_p$ ) circulation; (iv) the metabolic consumption  $M$ ; (v)  $[O_2]_a$  and  $R_s$  are modeled according to the previous description of the control mechanism. Note that we need not model these control systems in detail, but simply extract their most well-known features and use them to constrain the model.

In steady state the follow additional constraints hold:

$$\begin{aligned} Q_r &= Q_l = F_s = F_p \\ M &= F_s \cdot ([O_2]_a - [O_2]_v) \end{aligned} \quad [3]$$

The first equation is total blood circulation balance and the second one is based on the oxygen circulation balance, where

$F_s([O_2]_a - [O_2]_v)$  is the net change in the arterial and venous blood O<sub>2</sub> content. The oxygen drop  $\Delta O_2$  across the muscle bed is defined as  $\Delta O_2 = [O_2]_a - [O_2]_v$ . Combining 2 and 3 plus simple algebra (*SI Appendix*) gives the steady-state model  $(P_{as}, \Delta O_2) = f(H, W)$  shown in Fig. 3 that constrains the relationship between  $(P_{as}, \Delta O_2)$  and  $(H, W)$ .

In general the circulatory system is far from steady state in our experiments. Modeling the blood volume change for each circulatory compartment and the oxygen change in the tissue keeps the constraints from Eq. 2 but replaces 3 with the following dynamic model:

$$\begin{aligned} c_{as} \dot{P}_{as} &= Q_l - F_s \\ c_{vs} \dot{P}_{vs} &= F_s - Q_r \\ c_{ap} \dot{P}_{ap} &= Q_r - F_p \\ v_{T,O_2} \dot{[O_2]_v} &= -M + F_s \cdot ([O_2]_a - [O_2]_v) \\ c_{vp} \dot{P}_{vp} &= V_{total} - (c_{as} P_{as} + c_{vs} P_{vs} + c_{ap} P_{ap}). \end{aligned} \quad [4]$$

Here  $v_{T,O_2}$  denotes the effective tissue O<sub>2</sub> volume and we assume that tissues and venous blood gases are in equilibrium, namely that tissue oxygenation  $[O_2]_T$  is the same as venous oxygenation  $[O_2]_v$  (*SI Appendix*). The previous static analysis (and the purely static tradeoffs it highlights) directly extends to the dynamic case with modestly increased complexity. The simplest extension is to use an optimal linear quadratic state feedback controller (34) for linearizations of 4 at 0 and 100 W, with controller  $H = u(\cdot)$  chosen to minimize a weighted penalty on integrated elevation of  $P_{as}$ ,  $\Delta O_2$ , and  $H$ :

$$\min \int \left( q_p^2 (P_{as} - P_{as}^*)^2 + q_{O_2}^2 (\Delta O_2 - \Delta O_2^*)^2 + q_H^2 (H - H^*)^2 \right) dt \quad [5]$$

subject to linearizations of the state dynamic constraint 4. Fig. 4 compares HR and workload data versus simulations of applying the linear controllers to the model in 4 for two experiments

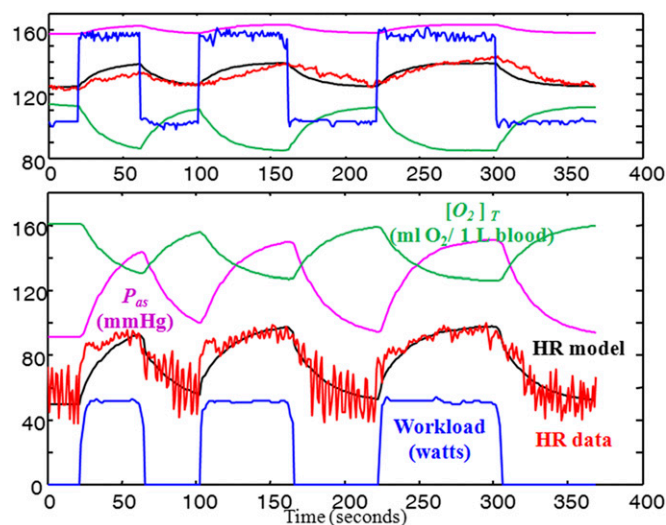


**Fig. 4.** Optimal control model response using first-principle model to two different workload (blue) demands, approximately square waves of 0–50 W (Lower) and 100–150 W (Upper): For each data set (using subject 2’s data), a physiological model with optimal controller is simulated with workload as input (blue) and HR (black) as output, and compared with collected HR data (red). Simulations of blood pressure ( $P_{as}$ , purple) and tissue oxygen saturation ( $[O_2]_T$ , green) are consistent with the literature but data were not collected from subjects. Breathing is spontaneous (not controlled).

(similar to Fig. 1 but with a different subject) with higher penalty on  $P_{as}$  and  $H$  at higher workloads as in the static case. (See [SI Appendix](#) for more details.) Also shown are simulations of  $P_{as}$  and  $[O_2]_T$ , which are consistent with the literature but were not measured. The same methods and results apply to other subjects' data and new experiments (e.g., cross-validation; see [SI Appendix](#)). Also note that for different subjects, we use the same nominal values for most parameters except the constants  $c_r, c_l$  used in the cardio-output formulation and the weighting parameters  $q_P, q_{O_2}, q_H$  used in the tradeoff function 5. The different  $c_r, c_l$  reflect the different sizes of subjects and different  $q_P, q_{O_2}, q_H$  reflect the qualitative differences in the control objectives.

The change in the tradeoff as workload increases is consistent with what we observed using the static model. At low workload and low HR, the main tradeoff is metabolic because both  $P_{as}$  and HR are at safe and sustainable levels. High HR and thus high  $[O_2]_T$ , (low  $\Delta O_2$ ), maintains aerobic muscle metabolism, extending the potential duration of exercise while preserving carbohydrate resources for the brain. At higher workloads, this strategy would produce unsustainably high and potentially damaging  $P_{as}$  and possibly HR, so the optimal controller penalizes these factors more, at the price of reduced  $[O_2]_T$ . HRV (slow time scale) in Fig. 1 (and  $P_{as}$  in Fig. 4) decreases with increasing workload because of the changing tradeoffs between metabolic overhead and  $P_{as}$ ,  $\Delta O_2$ , and  $H$  as their means increase. These explanations in HRV derived from the dynamic aerobic model are richer and more complete but due to the same tradeoffs as in the simpler static model.

Importantly, although the mathematics and physiology required are relatively elementary and the resulting explanation is

intuitively clear and mechanistic, they nonetheless highlight the rigor and scalability of this approach. The simplicity of the black-box fits in 1 and Fig. 1 helps establish causal relationships between variables and suggests physiological mechanisms to model in more detail, and highlights features in the signals that are not modeled (i.e., we have not explained the high frequency of the signals at low watts in Fig. 1, considered in the next sections). The hard homeostatic tradeoffs and the actuator effects of HR, ventilation, and vasodilation were included in the physiology model in 2–5 but the neuroendocrine implementation details were not. Also, the impact of cerebral autoregulatory saturation was included, but the details of implementation were not. Nonetheless, this approach allows for clinically actionable explanations that do not depend on poorly understood mechanisms peripheral to the component being modeled, and provides a framework for systematically refining such models using a similar (but presumably vastly more complex) combination of black- and gray-box models and physiology. Again, if new tradeoffs not considered here are found to be significant, they can be added directly as additional constraints are recognized and solutions recomputed. Further, tradeoffs may well change as organ systems fail, when these models are extended to disease states.

**High-Frequency HRV.** The high-frequency fluctuations in HR that are particularly large at low mean workloads and low HR cannot be explained by the simple fits or models above, and thus additional signals and mechanisms must be included that can be causally related to this setting. Figs. 5 and 6 shed light on breathing as a cause of much of the high-frequency HRV. Fig. 5A shows HR (red) during natural breathing at rest, with the

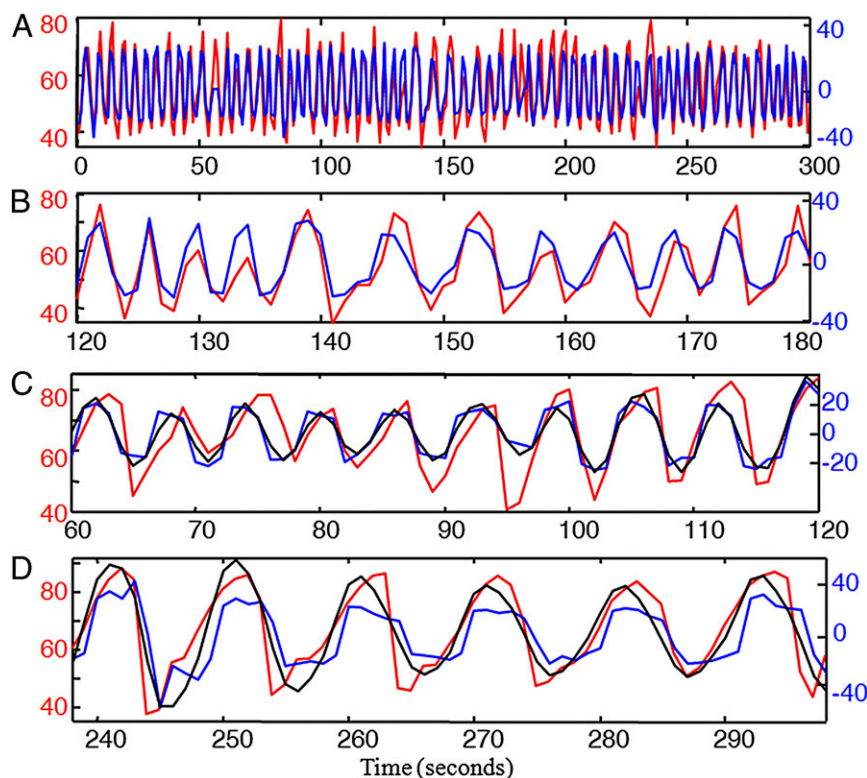


**Fig. 5.** HR response (red) to ventilation  $V$  (blue) at rest (0 W): The ventilatory data are raw speed of inhalation and exhalation measured at the mouthpiece. In each case the units for  $V$  (blue) are chosen to show the optimal static fit  $h(V) = b \cdot V + c$  to the collected HR data. A and B show natural breathing, with B zoomed in to focus on a smaller window to help visualize the data and fit. C and D are similar focused smaller windows from a longer controlled breathing experiment at resting (0 W) where the subject followed a frequency sweep from fast to slow breathing (see Fig. 6 for the full frequency range). C focuses on breathing frequencies close to natural breathing, whereas D focuses on frequencies slower than natural. Both C and D show simulated dynamic fits (black), and optimal static fits  $h(V) = b \cdot V + c$  (blue). The dynamic fits improve on the static fits more for the controlled sweep than for natural breathing (Table 2).



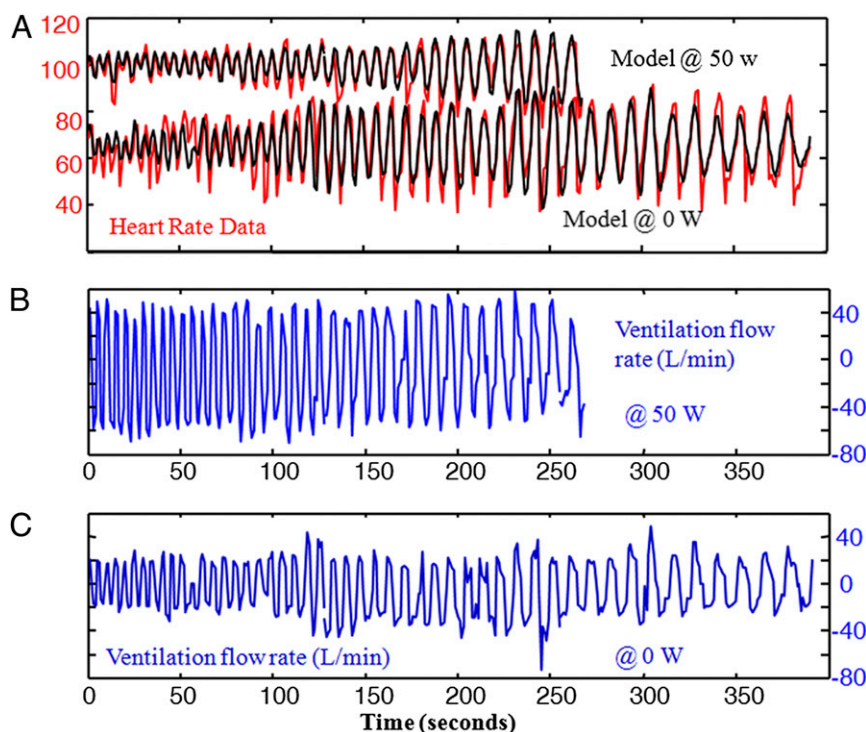


**Fig. 6.** HR response to sweep ventilation on different workload levels: Two experiments with (A) HR (red) and dynamic fit (black) to input of controlled ventilation frequency sweeps with measured ventilatory flow rate (blue) on a fixed background workload of (B) 0 W or (C) 50 W. Ventilatory flow (with spontaneous ventilation magnitude) was necessarily larger at 50 W and the subject was unable to breathe slowly enough to complete the entire frequency sweep.

optimal static fit  $H = h(V) = b \cdot V + c$ , where  $V$  (blue) is measured ventilation flow rates (inhalation and exhalation) at the mouth-piece. The static linear fit can be used to scale the units of  $V$  (blue) in Fig. 5A to visualize the best fit to HR (red) and its error, shown in Table 2. That HR and ventilation match so well in frequency is consistent with the observation that under certain conditions, inspiration is accompanied by an acceleration of HR, and expiration by a deceleration, a phenomenon called respiratory sinus arrhythmia (RSA) (16, 40–46). However, because ventilation and HR are both generated by neuroendocrine control, this fit (i.e., correlation) by itself does not suggest a specific mechanistic explanation of the resulting ventilation–HR correlation or HRV.

To sharpen this picture, Fig. 6 shows data from subjects instructed to control respiratory rate (RR, shown in blue) by following a computer-generated RR frequency sweep (tidal volumes not controlled), repeated with a background of 0- and 50-W exercises, respectively. (Fig. 5B shows HR and zoomed in for the 0-W exercise data.) For each exercise taken separately, HR is fit with static (blue in Fig. 5B) and one-state models, as well as a two-state, five-parameter linear model (shown in black in Figs. 5B and 6, Table 2):

$$\begin{aligned}\Delta H(t) &= a_1 H(t) + b_1 V(t) + x(t) \\ \Delta x(t) &= a_2 x(t) + b_2 V(t) + c\end{aligned}$$

where  $V$  is ventilatory flow rates,  $x$  is an internal black-box state, and the parameters depend on workload. Whereas breathing cannot be varied as systematically and widely as workload, these black-box fits provide strong evidence that ventilation is the main factor causing high-frequency HRV. The underlying physiological mechanisms remain unclear, but we now know where to look next. In Fig. 6, minute ventilation naturally increases at 50 W, yet HRV goes down, a nonlinear pattern consistent with the trends in Figs. 1 and 3, but more dramatic. As Table 2 shows, dynamic

fits have little benefit for natural breathing at rest, but modestly reduce the error for the controlled respiratory sweeps at low- and high-frequency breathing. In all cases, the frequency of HR oscillations is fit better than the magnitude, suggesting both a dynamic and nonlinear dependence of HR on ventilatory flow rates.

Although RSA magnitude has been used as a measure of vagal function, after many years of research the mechanism of RSA, e.g., whether RSA is due to a central or a baroreflex mechanism, is still debated (16, 40–46). Moreover, the data and dynamic fits show a small resonant peak in the frequency response at around 0.1 Hz at 0 W, and the significance of the peak is unclear. Of note, this characteristic peak occurred in the fits for every subject (although the exact RR at which it occurs varied), and is consistent with observations in the literature (16, 40). (In *SI Appendix*, we also use both workload and ventilation data as inputs to fit HR data during the easy workout in Fig. 1.)

Resolution of these mysteries requires additional measurements such as arterial blood pressure (more invasive human studies), more sophisticated physiological modeling including the mechanical effects of breathing on arterial blood pressure and pulmonary stretch reflexes, plus changing tradeoffs in control of arterial blood pressure at different workloads and HR levels. In particular, model 2–5 above assumed continuous ventilation and HRs (i.e., no intrabreath or -beat dynamics), so more detailed modeling of physiological respiratory patterns and their mechanical and metabolic effects is needed.

## Discussion

**Robust Efficiency and Actuator Saturation.** We showed how HR fluctuations in healthy athletes can be largely explained as nonlinear dynamic, but not chaotic, responses to either external (e.g., workload) or internal (e.g., ventilation implemented by pulsatile breathing) disturbance. We provided mechanistic explanations and plausible conjectures for essentially all of the HRV in Fig. 1, and showed that changes in HRV per se, no matter how mea-

**Table 2.** rms error for models of different complexity for data in Figs. 5 and 6

Row no.	No. prms	Model structure	Resting natural	Resting sweep	50-W sweep
1	0	Zero	56	67	98
2	1	Constant	11.6	13.1	7.9
3	2	Static	6.4	9.7	5.9
4	3	First-order dynamic	6.0	9.7	5.5
5	6	Second-order dynamic	6.0	7.5	4.0

Items in yellow highlight the best models balancing fitting error with model complexity.

sured, are much less important mechanistically than the tradeoffs that produce them. The tradeoffs we highlight between robustness, homeostasis, and metabolic efficiency are universal and essential (1, 23) features of complex systems but can remain hidden and cryptic (47) without an appropriate mathematical framework (4, 48). “Universal” features illustrated by this physiological (HR) control system include how efficiently maintaining robust homeostasis (e.g., small errors in CBF,  $S_aO_2$ , and  $\Delta O_2$ ) in the presence of large disturbances requires correspondingly large actuator (e.g., HR, ventilation, and cerebral autoregulation) responses to compensate, and how nonlinearities in actuator saturations lead to reductions in actuator activity (e.g., HRV) under increased load or stress.

HR control and HRV highlight layered control, actuator constraints, and hard tradeoffs of the type that pervade physiology and are generally fundamental in complex control systems. In summary, actuators are the mechanisms by which controllers act on the system to provide efficient performance and robust homeostasis. In the cardiovascular models so far, the most important saturation is in cerebral autoregulation, which forces a nonlinear change in  $H = h(W)$  as workload increases to avoid high  $P_{as}$  that leads to intracerebral pathology (edema, hemorrhagic stroke).

Further understanding of control complexity and the role of actuator (e.g., HR) variability and saturation in physiologic control comes from examination of other technological examples of complex systems. Familiar examples include automobiles, particularly new autonomous robotic versions. A car is moved and controlled via the actuators that produce and deliver power, braking, and steering that result in accelerations in forward, backward, and lateral directions. Most complexity in an autonomous robot car is in the control system for robust efficiency to uncertainty in real traffic environments and to intrinsic variability in components. If scientists were forced to “reverse engineer” such a car without access to the forward engineering process, they would likely study “knockouts” of components to infer their function, and also push the vehicles to extremes to find the limits of their robust performance. It would be surprising if “reverse engineering” cardiovascular control would be easier than a robot car, or could be accomplished with less sophisticated tools and without domain-specific details.

Loss of car actuator variability due to “stress” parallels loss of HRV, in that it is loss of actuator responsiveness that causes deterioration of function, and loss of variability is only a symptom of actuator dysfunction. Currently, human drivers cause most crashes when they reduce their actuator responsiveness because of multitasking, alcohol consumption, fatigue, or poor visibility, or when surface conditions make the actuators less effective. Automatic collision avoidance and antilock and anti-slip traction control systems mitigate these effects, and augment human control in emergencies. However, even in fully automated robotic cars with robust control systems, at extremes of speed, acceleration, braking, and turning (such as a race scenario or in icy conditions), actuators would frequently saturate and lose variability, resulting in less maneuverability, and an increase in errors and risk of crashes. Thus, actuator saturation causing changes in variability is a “signature” of a wide variety of dan-

gerous scenarios, and essential to understanding vehicle limits and malfunction. However, variability per se is unimportant, and analyzing the statistics of individual signals (e.g., fuel or air rates, braking, acceleration, turning rate, etc.) in isolation is relatively less diagnostic compared with understanding integrated, mechanistic dynamic models of signal interactions.

Similar tradeoffs to those resulting in HRV are found throughout technology and biology. For example, glycolytic oscillations were one of the most persistent mysteries involving dynamics in cell biology (1). The proximal role of how autocatalytic and regulatory feedbacks make oscillations possible was well understood, but the unresolved deeper “why” question was the purpose of the oscillations, or alternatively, whether they were just frozen accidents of evolution. Oscillations are neither functional nor accidental but are a side effect of provably hard tradeoffs involving efficiency and robust control (1). The glycolysis circuit must maintain adequate ATP concentrations that are robust to fluctuations in demand and to enzyme and other metabolite levels. It must also be metabolically efficient, in the sense of not requiring excessive enzyme concentrations. Any circuit that aims to balance these competing requirements has the potential to oscillate, particularly when enzymes saturate.

**Mathematical Framework.** It has been difficult to characterize multilayered aspects of biological control, but our approach is aimed at providing tools for biologists and clinicians, combining established principles of system identification fits and control theory with basic physiological models. The fits in Figs. 1, 5, and 6 highlight causal input–output relationships between variables and help suggest the relevant physiology. By comparison, even the most sophisticated statistical analysis of individual HR signals taken out of physiologic context is mechanistically uninformative. In contrast, the static and dynamic models mechanistically explain Figs. 3 and 4 and most of the variability in Fig. 1 (i.e., the black curves at the lower two watts). Our explanation in terms of aerobic metabolism is simple and intuitive as well as mechanistic, and requires only basic mathematics and physiology. The main requirement of the models is some mechanistic relationship between control actuation and its limits in maintaining robust homeostasis. Thus, we did not need detailed understanding of neuroendocrine control implementation or peripheral autoregulation, but only that they adequately manage the tradeoffs and saturation effects in muscle, brain, and heart as described above. Moreover, specific details of the computational approach, e.g., piecewise linear least squares used in this paper, are not essential to understanding the underlying system control. What is important is that the right constraints are properly reflected in the computation, so that the resulting controller function is constrained by the right physiological mechanisms plus appropriately changing penalties–constraints on vital physiological variables due to metabolic tradeoffs and limit.

Our approach also importantly highlights where mechanisms are missing. The model in 2–5 and Fig. 4 assume continuous ventilation and HRs (i.e., no intrabreath or -beat dynamics) and do not capture any of the higher frequency HRV in Fig. 1. The fits in Figs. 5 and 6 suggest that the dynamics of physiological respiratory patterns and their mechanical and metabolic effects



are necessary and perhaps sufficient to explain the high-frequency HRV seen in Fig. 1. There may also be connections between robust efficiency and oscillations as in ref. 1 to explain the origin of the peaks in frequency response of the breath-to-HR fits.

An essential feature of this project is that our tools be robust and scalable to more complex signals and models, and that if new mechanisms and/or tradeoffs are discovered that are important, they can be added as additional constraints. Fortunately, we can leverage enormous recent advances in engineering theory and practice, although these remain largely unknown in mainstream science outside of the most advanced parts of systems biology. The general models and methods, particularly moving from 1 to 2–5 (and Fig. 1 to Figs. 3 and 4), used for this relatively straightforward study should serve well as a foundational framework for the evaluation of even more complex physiologic (disease) situations in which the diagnostic possibilities are broader.

**Clinical Correlates: Linking the Behavior of Control Systems and Pathophysiology.** Clinicians know that changes in actuator signals (e.g., HR increases) can signify a great variety of potentially important derangements such as hypovolemia, congestive heart failure, inflammation, sepsis, etc. (6–13). Even without specific diagnostic content, alerts to clinicians that HRV is changing can be useful. Such an alert has been incorporated into monitoring of premature neonates. In this case, monitoring of HR characteristics is used to report a statistic that reflects the performance of the actuator mechanisms. The utilization of this statistic by clinicians was sufficient to change practice (i.e., reevaluation of the patient with consideration of need for additional therapies) and achieve a significant improvement in outcomes (10, 13). This particular example of integration of mathematical analysis into monitors represents a special situation because the alert also incorporates the occurrence of cardiac decelerations, a phenomenon not observed in adults. Furthermore, because sepsis is a common problem in this setting, the clinicians chose to administer antimicrobial therapy on the basis of the alert which produced the outcome benefit. In fact, the efficacy of the monitor in early sepsis detection was subsequently demonstrated in a post hoc analysis (13). However, in most clinical scenarios, actuator changes alone are usually so generic that they lack specific diagnostic value, and extensive analyses of individual time series have not yielded mechanistic explanations that can narrow the diagnosis (6–12).

In contrast, the general type of models and methods used here and the application of control theory to physiology present an

enormous opportunity to reexamine this area with powerful mathematical tools and a systems engineering approach (48). This is important because system dysfunction is manifested earlier in the behavior of the control system than in any metric associated with the system's output. The long-term goal of this research is earlier diagnosis afforded by monitoring control elements in addition to individual signal outputs.

## Materials and Methods

After Caltech Institutional Review Board approval, five fit athletic subjects (ages 25–35 y, three men and two women) performed a series of experimental exercise regimens, each on two different days. The intensity and durations were less than routine training for these athletes, and they had used the laboratory equipment before so were familiar and comfortable with the environment. In all experiments, the subject pedaled a Life Fitness stationary recumbent bicycle at near-constant speed with the pedaling resistance controlled by a preprogrammed protocol. In the respiration rate (RR) sweep experiments, a sinusoid signal was preprogrammed in the computer with frequency from 2 Hz to 0.06 Hz and each subject watched the signal and controlled RR to follow the frequency of the signal until they were unable to continue.

In all exercise tests, 1-Hz work rate data were recorded from a Life Fitness stationary recumbent exercise bicycle interfaced with a computer running MATLAB via the Communications Specification for Fitness Equipment protocol. Other exercise testing data were collected using commercially available noninvasive monitors. (i) RR interval HR data were recorded with a Polar heart rate monitor and converted to 1-Hz HR data using the integral pulse frequency modulation model (49). (ii) In the tests shown in Figs. 5 and 6, 100-Hz ventilation (inhalation and exhalation) flow rate data were recorded with a Philips NiCO<sub>2</sub> monitor, and down-sampled to 1-Hz ventilation flow rate data. (iii) In the test shown in Fig. 7, 1-Hz gas data including minute ventilation  $\dot{V}_E$ , oxygen consumption  $\dot{V}O_2$  and carbon dioxide generation  $\dot{V}CO_2$  were collected with a Vacumetrics monitor and TurboFit software. No other preprocessing of data was performed.

A detailed discussion of mathematical methods is given in [SI Appendix](#).

**ACKNOWLEDGMENTS.** We thank Pamela B. Pesenti for her gift in establishing the John G. Braun Professorship, which supported this research, and Philips for providing equipment used in the experiments. The research progress has been presented and discussed at several meetings, including the International Conference on Complexity in Acute Illness of the Society for Complexity in Acute Illness (SCAI). Comments from many SCAI members greatly influenced this paper. We also thank the athletes who were the subjects for this study. The theoretical aspects of this work and the connections with other complex systems challenges were supported in part by Air Force Office of Scientific Research and National Science Foundation. Preliminary exploration in this research direction was funded by Pfizer, National Institutes of Health (R01 GM078992), and the Institute of Collaborative Biotechnologies (ARO W911NF-09-D-0001).

- Chandra FA, Buzi G, Doyle JC (2011) Glycolytic oscillations and limits on robust efficiency. *Science* 333(6039):187–192.
- Pool R (1989) Is it healthy to be chaotic? *Science* 243(4891):604–607.
- Buzsáki G (2006) *Rhythms of the Brain* (Oxford Univ Press, New York).
- Glass L (2001) Synchronization and rhythmic processes in physiology. *Nature* 410(6825):277–284.
- Buchman TG (2002) The community of the self. *Nature* 420(6912):246–251.
- Goldberger AL, et al. (2002) Fractal dynamics in physiology: alterations with disease and aging. *Proc Natl Acad Sci USA* 99(Suppl 1):2466–2472.
- Camm AJ, et al.; Task Force of the European Society of Cardiology and the North American Society of Pacing and Electrophysiology (1996) Heart rate variability: Standards of measurement, physiological interpretation and clinical use. *Circulation* 93(5):1043–1065.
- Ivanov PC, et al. (1999) Multifractality in human heartbeat dynamics. *Nature* 399(6735):461–465.
- Poon CS, Merrill CK (1997) Decrease of cardiac chaos in congestive heart failure. *Nature* 389(6650):492–495.
- Moorman JR, et al. (2011) Cardiovascular oscillations at the bedside: Early diagnosis of neonatal sepsis using heart rate characteristics monitoring. *Physiol Meas* 32(11):1821–1832.
- Tulppo MP, Mäkelä TH, Takala TE, Seppänen T, Huikuri HV (1996) Quantitative beat-to-beat analysis of heart rate dynamics during exercise. *Am J Physiol* 271(1 Pt 2):H244–H252.
- Yamamoto Y, Hughson RL, Peterson JC (1991) Autonomic control of heart rate during exercise studied by heart rate variability spectral analysis. *J Appl Physiol* (1985) 71(3):1136–1142.
- Moorman JR, et al. (2011) Mortality reduction by heart rate characteristic monitoring in very low birth weight neonates: A randomized trial. *J Pediatr* 159(6):900–906.e1.
- Akselrod S, et al. (1981) Power spectrum analysis of heart rate fluctuation: A quantitative probe of beat-to-beat cardiovascular control. *Science* 213(4504):220–222.
- Mackey MC, Glass L (1977) Oscillation and chaos in physiological control systems. *Science* 197(4300):287–289.
- Novak V, et al. (1993) Influence of respiration on heart rate and blood pressure fluctuations. *J Appl Physiol* 74(2):617–626.
- Gieraltowski J, Żebrowski JJ, Baranowski R (2012) Multiscale multifractal analysis of heart rate variability recordings with a large number of occurrences of arrhythmia. *Phys Rev E Stat Nonlin Soft Matter Phys* 85(2 Pt 1):021915.
- Barabási AL (2009) Scale-free networks: A decade and beyond. *Science* 325(5939):412–413.
- Glass L (2009) Introduction to controversial topics in nonlinear science: Is the normal heart rate chaotic? *Chaos* 19(2):028501.
- Kluttig A, Kuss O, Greiser KH (2010) Ignoring lack of association of heart rate variability with cardiovascular disease and risk factors: Response to the manuscript “The relationship of autonomic imbalance, heart rate variability cardiovascular disease risk factors” by Julian F. Thayer, Shelby S. Yamamoto, Jos F. Brosschot. *Int J Cardiol* 145(2):375–376.
- Young NS, Ioannidis JPA, Al-Ubaydli O (2008) Why current publication practices may distort science. *PLoS Med* 5(10):e201.
- Stumpf MPH, Porter MA (2012) Mathematics. Critical truths about power laws. *Science* 335(6069):665–666.
- Alderson DL, Doyle JC (2010) Contrasting views of complexity and their implications for network-centric infrastructures. *IEEE Transactions on Systems, Man and Cybernetics, Part A: Systems and Humans* 40(4):839–852.
- Ioannidis JPA (2005) Why most published research findings are false. *PLoS Med* 2(8):e124.

25. Wiggert O (1970) Dynamics of ventilation and heart rate in response to sinusoidal work load in man. *J Appl Physiol* 29(2):208–218.
26. Warner HR, Cox A (1962) A mathematical model of heart rate control by sympathetic and vagus efferent information. *J Appl Physiol* 17(2):349–355.
27. Brooks GA, Fahey TD, Baldwin K (2004) *Exercise Physiology: Human Bioenergetics and Its Applications* (McGraw-Hill, New York).
28. Rowell LB (1993) *Human Cardiovascular Control* (Oxford Univ Press, New York).
29. Grodins FS, Buell J, Bart AJ (1967) Mathematical analysis and digital simulation of the respiratory control system. *J Appl Physiol* 22(2):260–276.
30. Guyton A, Hall J (2006) *Textbook of Medical Physiology* (Elsevier Saunders, Philadelphia), 11th Ed.
31. Hoppensteadt FC, Peskin CS (2002) *Modeling and Simulation in Medicine and the Life Sciences* (Springer, New York).
32. Batzel JJ, Schneiditz D (2007) *Cardiovascular and Respiratory Systems: Modeling, Analysis, and Control* (Society for Industrial and Applied Mathematics, Philadelphia).
33. Ljung L (1999) *System Identification: Theory for the User* (Prentice Hall, Upper Saddle River, NJ).
34. Kirk D (2004) *Optimal Control Theory: An Introduction* (Dover, New York).
35. Doya K, Ishii S, Pouget A, Rao RPN, eds. (2007) *Bayesian Brain: Probabilistic Approaches to Neural Coding*. (MIT Press, Cambridge, MA).
36. Cheng TM, Savkin AV, Celler BG, Su SW, Wang L (2008) Nonlinear modeling and control of human heart rate response during exercise with various work load intensities. *IEEE Trans Biomed Eng* 55(11):2499–2508.
37. Mullen TJ, Appel ML, Mukkamala R, Mathias JM, Cohen RJ (1997) System identification of closed-loop cardiovascular control: Effects of posture and autonomic blockade. *Am J Physiol* 272(1 Pt 2):H448–H461.
38. Paulson OB, Strandgaard S, Edvinsson L (1990) Cerebral autoregulation. *Cerebrovasc Brain Metab Rev* 2(2):161–192.
39. Bramble DM, Lieberman DE (2004) Endurance running and the evolution of Homo. *Nature* 432(7015):345–352.
40. Mehlsen J, Pagh K, Nielsen JS, Sestoft L, Nielsen SL (1987) Heart rate response to breathing: Dependency upon breathing pattern. *Clin Physiol* 7(2):115–124.
41. Hirsch JA, Bishop B (1981) Respiratory sinus arrhythmia in humans: How breathing pattern modulates heart rate. *Am J Physiol* 241(4):H620–H629.
42. Eckberg DL (1983) Human sinus arrhythmia as an index of vagal cardiac outflow. *J Appl Physiol* 54(4):961–966.
43. Schäfer C, Rosenblum MG, Kurths J, Abel HH (1998) Heartbeat synchronized with ventilation. *Nature* 392(6673):239–240.
44. Grossman P, Karemaker J, Wieling W (1991) Prediction of tonic parasympathetic cardiac control using respiratory sinus arrhythmia: The need for respiratory control. *Psychophysiology* 28(2):201–216.
45. Berntson GG, Cacioppo JT, Quigley KS (1993) Respiratory sinus arrhythmia: Autonomic origins, physiological mechanisms, and psychophysiological implications. *Psychophysiology* 30(2):183–196.
46. Eckberg DL (2009) Point:counterpoint: Respiratory sinus arrhythmia is due to a central mechanism vs. respiratory sinus arrhythmia is due to the baroreflex mechanism. *J Appl Physiol* (1985) 106(5):1740–1742, discussion 1744.
47. Doyle JC, Csete M (2011) Architecture, constraints, and behavior. *Proc Natl Acad Sci USA* 108(Suppl 3):15624–15630.
48. Winslow RL, Trayanova N, Geman D, Miller MI (2012) Computational medicine: Translating models to clinical care. *Sci Trans Med* 4(158):158r111.
49. Han K, Nagel JH, Schneiderman N (1992) A continuous representation of heart rate. *Engineering in Medicine and Biology Society, 1992. 14th Annual International Conference of the IEEE* 2:785–786.